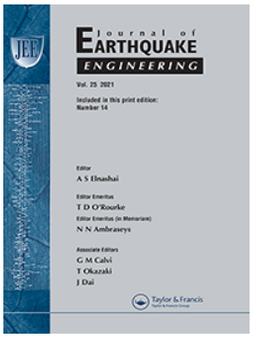

Journal of Earthquake Engineering

ISSN: (Print) (Online) Journal homepage: https://www.tandfonline.com/loi/ueqe20

Damping Modification Factor of Acceleration Response Spectrum considering Seismological Effects

Haizhong Zhang & Yan-Gang Zhao

To cite this article: Haizhong Zhang & Yan-Gang Zhao (2021): Damping Modification Factor of Acceleration Response Spectrum considering Seismological Effects, Journal of Earthquake Engineering, DOI: 10.1080/13632469.2021.1991521

To link to this article: https://doi.org/10.1080/13632469.2021.1991521

JOURNAL OF EARTHQUAKE ENGINEERING
https://doi.org/10.1080/13632469.2021.1991521

Taylor & Francis
Taylor & Francis Group

Damping Modification Factor of Acceleration Response Spectrum considering Seismological Effects

Haizhong Zhang and Yan-Gang Zhao

Department of Architecture, Kanagawa University, Yokohama, Japan

ABSTRACT

Although seismological effects on the damping modification factor of an acceleration response spectrum (DMF*a*) are important, seismological parameters in existing formulations are generally not specified in seismic codes. This study aims to propose a practical DMF*a* formulation using parameters available from seismic codes to reflect the seismological effects. To this end, an analytical approach is developed to explore the seismological effects on DMF*a*. It is found that a bandwidth factor defined as the ratio of acceleration spectral values at 6 and 0s can appropriately reflect the seismological effects, and thus is incorporated into the proposed DMF*a* formulation for seismic design.

ARTICLE HISTORY
Received 5 February 2021
Accepted 24 September 2021

KEYWORDS
Damping modification factor; acceleration response spectrum; seismological effects; bandwidth factor; seismic design

1. Introduction

The acceleration response spectrum has been used as a popular tool to assess the seismic demand of a building. Most seismic regulations specify the response spectral values corresponding to a standard damping ratio of 5%. To design structures with inherent damping ratios other than 5%, e.g., base-isolated structures (Naeim and Kelly 1999) or structures with supplementary damping devices (Constantinou, Soong, and Dargush 1998), the damping modification factor is considered the most effective tool.

In the past few decades, numerous studies have been conducted to understand the damping modification factor (DMF), and many simple formulations have been developed based on different databases of seismic records (Ashour 1987; Bommer and Elnashai 1999; Bommer and Mendis 2005; Cameron and Green 2007; Conde-Conde and Benavent-Climent 2019; Greco, Fiore, and Briseghella 2018b; Greco et al. 2018a, 2019; Hao et al. 2011; Hatzigeorgiou 2010; Hubbard and Mavroeidis 2011; Lin 2007; Lin and Chang 2003, 2004; Lin, Miranda, and Chang 2005; Mentrasti 2008; Mollaioli, Liberatore, and Lucchini 2014; Nagao and Kanda 2015; Newmark and Hall 1982; Palermo, Silvestri, and Trombetti 2016; Pu et al. 2016; Ramirez et al. 2000; Rezaeian et al. 2014; Sadek, Mohraz, and Riley 2000; Stafford, Mendis, and Bommer 2008; Tolis and Faccioli 1999; Xiang and Huang 2019; Zhao et al. 2019; Zhou et al. 2014). Castillo and Ruiz (2014) also developed a DMF formulation based on uniform hazard spectra. Most of these formulations were concerned with the pseudo-acceleration response spectrum, *Spa*, which is approximated from the displacement response spectrum. The pseudo-acceleration response spectrum, *Spa*, is suitable when the restoring force is of interest, such as in the design of a structure whose damping is mainly derived from supplementary damping devices (Lin and Chang 2003). However, the true acceleration response spectrum, *Sa*, is more suitable when the inertial force of the structure is of interest. Moreover, *Sa* and *Spa* can be substantially different especially in structures with large damping ratios and long periods (Lin and Chang 2003; Mentrasti 2008; Sadek, Mohraz, and Riley 2000). Therefore, it is necessary to develop a formulation for the DMF of *Sa* (DMF*a*) in seismic design.

Lin and Chang (2004) developed a formula for the DMF*a* based on statistical analyses of the ground-motion records for the United States. This formulation considered the effects of structural parameters, namely the structural period and damping ratio, as well as site conditions. Hatzigeorgiou

CONTACT Yan-Gang Zhao zhao@kanagawa-u.ac.jp Department of Architecture, Kanagawa University, Yokohama, Japan

(2010) developed a DMF*a* formulation based on statistical analyses of the universally recorded and artificial accelerograms; this formulation further incorporates the effects of the fault distance and type of earthquake motions (natural or artificial). Nagao and Kanda (2015) proposed a DMF*a* formula using several ground-motion records from earthquakes that occurred in Japan. This formulation incorporates the structural parameters and the standard deviation of the phase difference of earthquake motions. Pu et al. (2016) developed a formula for near-fault motions based on statistical analyses of pulse-like signals, including the structural parameters and pulse period. Conde-Conde and Benavent-Climent (2019) developed a DMF*a* formula based on European seismic records by considering the effects of structural parameters and duration of ground motion. Although these studies all agree upon the importance of the seismological effects on the DMF*a*, most of the seismological parameters in existing formulations, e.g., fault distance and standard deviation of phase difference, are generally not specified as part of the earthquake actions in seismic codes. Therefore, it is not feasible to directly apply these formulations incorporating the seismological parameters in a practical seismic design.

This study aims to propose a DMF*a* formulation using parameters available from seismic codes to reflect the seismological effects, which can be applied in practical seismic design. The remainder of this paper is organized as follows. First, existing formulations for the DMF*a* are briefly reviewed in Section 2. In Section 3, an analytical approach is developed based on random vibration theory (RVT) to explore the seismological effects on DMF*a*. In Section 4, the developed approach is verified by comparing with the results of the time-series analysis. In Section 5, seismological effects on DMF*a* are systematically explored, and an appropriate factor for seismic design is derived to reflect the seismological effects. In Section 6, a simple DMF*a* formulation adopting the derived factor is further proposed for a practical seismic design. Finally, conclusions of this study are presented in Section 7.

2. Existing DMF*a* Formulations

Although numerous formulations for the DMF of *Spa*, DMF*d*, have been developed, there are very few reported works for the DMF*a*. Lin and Chang (2004) developed a formula for the DMF*a* based on statistical analyses of 1,037 ground-motion records from 102 earthquakes that occurred in the United States. Their formula considered the effects of the structural period T_0, damping ratio ξ, and site conditions, and can be expressed as

$$\mathrm{DMF}a(T_0,\xi) = d + eT_0 \tag{1}$$

where d and e are coefficients depending on the soil type, as listed in Table 4 of Lin and Chang (2004). The site class in the study by Lin and Chang (2004) was defined according to the NEHRP (2000). Equation (1) is applied to $T_0 \geq 0.15$ s for site Class AB and $T_0 \geq 0.2$ s for site Classes C and D; DMFa = 1.0 for $T_0 = 0$ s for the three site classes. Values of the DMFa for 0 s < T_0 < 0.15 s (site Class AB) and 0 s < T_0 < 0.2 s (site Classes C and D) can be obtained by linear interpolation, and this formula is valid for damping ratios between 2% and 50% and oscillator periods up to 6 s.

Hatzigeorgiou (2010) developed another DMF*a* formulation based on the nonlinear regression analysis of 210 universally recorded and 100 artificial accelerograms. This formulation further incorporates the effects of the fault distance and type of earthquake motions (natural and artificial) and is expressed as

$$\begin{aligned}\mathrm{DMF}a(T_0,\xi) = {} & 1 + (100\xi - 5)[1 + c_1 \ln(100\xi) + c_2(\ln(100\xi))^2] \\ & \times [c_3 + c_4 ln(T_0) + c_5(ln(T_0))^2]\end{aligned}$$

where c_1–c_5 are coefficients depending on the soil type, fault distance, and type of earthquake motion (natural or artificial), as listed in Table VI of Hatzigeorgiou (2010); the site classes used in this study were defined according to the United States Geological Survey. This formula is valid for damping ratios between 0.5% and 50%, with oscillator periods up to 5 s.

Nagao and Kanda (2015) developed a DMF*a* formula based on a linear regression analysis of ground-motion records from 13 earthquakes in Japan. Their formula incorporates the structural parameters as well as the standard deviation of phase difference of earthquake motions, σ, and is expressed as

$$\mathrm{DMF}a(T_0,\xi) = a_{i,j} + b_{i,j}\sigma \tag{3}$$

where $a_{i,j}$ and $b_{i,j}$ are coefficients depending on the structural period and damping ratio, as presented in Table 2 of Nagao and Kanda (2015).

Pu et al. (2016) developed an expression for near-fault motions based on statistical analyses of 50 carefully selected pulse-like near-fault ground motions. This formula includes structural parameters as well as the pulse period T_p, and the DMF*a* is expressed in terms of the DMF*d*:

$$\mathrm{DMF}a(T_0,\xi) = \mathrm{DMF}d(T_0,\xi)\sqrt{\frac{1+4\xi^2\left(\frac{T_0}{T_p}+0.2\right)^2}{1+0.01\left(\frac{T_0}{T_p}+0.2\right)^2}} \tag{4-1}$$

When $T_0/T_p \geq .5$, the DMF*d* is expressed as

$$\mathrm{DMF}d(T_0,\xi) = \sqrt{\frac{\left[1-\left(\frac{T_0}{T_p}+0.2\right)^2\right]^2 + 0.55\left(\frac{T_0}{T_p}+0.2\right)^3}{\left[1-\left(\frac{T_0}{T_p}+0.2\right)^2\right]^2 + 5(\xi+0.06)\left(\frac{T_0}{T_p}+0.2\right)^3}} \tag{4-2}$$

When $0.01 < T_0/T_p < .5$, the DMF*d* is expressed as

$$\mathrm{DMF}d(T_0,\xi) = 1 + \frac{\log\frac{T_0}{T_p}+2}{1.699}\left(\sqrt{\frac{1}{0.81+3.82\xi}}-1\right) \tag{4-3}$$

When $T_0/T_p \leq .01$, the DMF*d* is expressed as

$$\mathrm{DMF}d(T_0,\xi) = 1 \tag{4-4}$$

Conde-Conde and Benavent-Climent (2019) developed a DMF*a* expression based on the European seismic records. Their formula considered the effects of the structural parameters and significant duration of ground motions, $D_{5\text{-}95\%}$, it is also expressed in terms of the DMF*d*:

$$\mathrm{DMF}a(T_0,\xi) = \mathrm{DMF}d(T_0,\xi) + \varepsilon\xi^{\lambda}T_0 \tag{5-1}$$

where the DMF*d* is expressed as

$$\mathrm{DMF}d(T_0,\xi) = \left[1+\left(\sqrt{\frac{0.05+\xi}{0.10}}-1\right)\left(\frac{T_R}{T_0}\right)^{a^{\frac{T_0-T_R}{T_0}}}\right]^{-1} \tag{5-2}$$

Here, λ, ε, T_R, and a are coefficients depending on the soil type and significant duration of ground motions $D_{5\text{-}95\%}$, as listed in Table 4 of Conde-Conde and Benavent-Climent (2019). Further, the site class in this study was defined according to Eurocode 8 (2004), and the formula is valid for damping ratios between 10% and 90%, with oscillator periods up to 4 s.

All of the aforementioned studies as well as others exploring the seismological effects (Hao et al. 2011; Zhao et al. 2019) agree that the DMF*a* could be significantly affected by seismological parameters; these studies incorporate various seismological parameters into the DMF*a* formulations. However, the incorporated seismological parameters, e.g., fault distance, standard deviation of the phase difference, pulse period, and ground-motion duration, are generally not specified as part of the seismic design actions in seismic codes. Therefore, it is not feasible to directly apply these formulations incorporating said seismological parameters in a practical seismic design.

3. Analytical Approach for the DMF*a*

To develop a DMF*a* formulation considering the seismological effects for a practical seismic design, it is necessary to find an appropriate factor that is available from seismic codes to reflect the seismological effects. To this end, this section presents an analytical approach for DMF*a* to systematically explore the seismological effects and theoretically clarify the factor essentially governing the seismological effects. In particular, to involve various seismological parameters, a source-based Fourier amplitude spectrum (FAS) model is used to characterize the ground motions. Then, the random vibration theory (RVT) is applied to evaluate the DMF*a* by considering its ability to easily relate the FAS to the response spectrum (Zhang and Zhao 2020).

3.1. Earthquake Ground-motion Model

To investigate the seismological effects on the DMF*a*, it is desirable to characterize the earthquake ground motions through a source-based model that includes various seismological parameters, such as the magnitude, distance, and site conditions. The simplest source-based model involves using the seismological theory to compute the radiated FAS from a point source in terms of the source, path, and site parameters (EPRI 1993). This study utilizes the FAS model described by Boore (1983, 2003), which has been adequately validated via comparisons with observations from real ground motion records (1983, 2003). The FAS of ground acceleration, $Ya(f)$, is expressed as the product of the source term $E(M_0, f)$, propagation path term $P(R, f)$, and site term $G(f)$, as

$$Ya(f) = E(M_0, f) \times P(R, f) \times G(f) \tag{6}$$

where f denotes the frequency, R denotes the distance from site to the source, and M_0 denotes the seismic moment, which is related to the moment magnitude M as

$$M_0 = 10^{1.5M+10.7} \tag{7}$$

The Brune omega-squared point-source spectrum (Brune 1970, 1971) is most commonly used to represent the radiated FAS from an earthquake. This source spectrum can be coupled with the path and site terms defined by Boore (1983, 2003) to obtain

$$Ya(f) = \left[0.78\frac{\pi}{\rho\beta^3}M_0\frac{f^2}{1+(f/f_c)^2}\right]\left[Z(R)\exp\left(\frac{-\pi fR}{Q(f)\beta}\right)\right][\exp(-\pi\kappa f)A(f)] \tag{8}$$

where, ρ and β denote the density and shear wave velocity of the crust, respectively, $Z(R)$ denotes the geometric attenuation, κ denotes the site diminution, $Q(f)$ denotes the anelastic attenuation, and $A(f)$ denotes the crust amplification. Further, f_c is the corner frequency representing the frequency below which the FAS decays and is defined as

$$f_c = 4.9 \times 10^6 \beta(\Delta\sigma/M_0)^{1/3} \tag{9}$$

where $\Delta\sigma$ is the stress drop. Typical values of the seismological parameters required in Equations. (8) and (9) are determined based on Boore and Thompson (2015), as detailed in Table 1 of Wang and Rathje (2016).

3.2. Expression for DMF*a*

To estimate the DMF*a* using the FAS, the random vibration theory (RVT) is applied considering its ability to easily relate the FAS to the response spectrum. Based on the RVT, Boore (1983, 2003) derived an expression for the pseudo-acceleration response spectrum *Spa*, i.e., $Spa(\bar{\omega}, \xi)$, from the FAS, which is expressed as

$$Spa(\bar{\omega},\xi)=\overline{pf}_{\xi}\sqrt{\frac{1}{D_{rms,\xi}\pi}\int_{0}^{\infty}|YR(\omega,\bar{\omega},\xi)|^{2}d\omega} \tag{10}$$

where $\bar{\omega}$ and ξ are the circular frequency and damping ratio for a single-degree-of-freedom oscillator, respectively, $D_{rms,\xi}$ and $\overline{pf}_{\xi}$ are the duration and expected value of the peak factor of the oscillator response, respectively, and $YR(\omega,\bar{\omega},\xi)$ represents the oscillator-response FAS, which is obtained from FAS of the ground acceleration $Ya(\omega)$ as

$$YR(\omega,\bar{\omega},\xi)=Ya(\omega)|Hpa(\omega,\bar{\omega},\xi)| \tag{11}$$

In Equation (11), $Hpa(\omega,\bar{\omega},\xi)$ is the oscillator transfer function for the pseudo-acceleration and is given by

$$|Hpa(\omega,\bar{\omega},\xi)|=\frac{1}{\sqrt{(2\xi\omega/\bar{\omega})^{2}+((\omega/\bar{\omega})^{2}-1)^{2}}} \tag{12}$$

This study focuses on the true acceleration response spectrum, $Sa(\bar{\omega},\xi)$, instead of the pseudo one, $Spa(\bar{\omega},\xi)$. Based on the RVT, $Sa(\bar{\omega},\xi)$ can be obtained using Equation (10) by replacing the oscillator transfer function $Hpa(\omega,\bar{\omega},\xi)$ for the pseudo-acceleration with that for the true acceleration. The oscillator transfer function for the true acceleration, $Ha(\omega,\bar{\omega},\xi)$, is expressed as

$$|Ha(\omega,\bar{\omega},\xi)|=\frac{\sqrt{(2\xi\omega/\bar{\omega})^{2}+1}}{\sqrt{(2\xi\omega/\bar{\omega})^{2}+((\omega/\bar{\omega})^{2}-1)^{2}}} \tag{13}$$

As most seismic codes only specify the pseudo-acceleration spectrum of a damping ratio of 5% $Spa(\bar{\omega},5\%)$, in order to obtain the true acceleration spectrum corresponding to an arbitrary damping ratio ξ, $Sa(\bar{\omega},\xi)$, it is more reasonable to define the DMF*a* as the ratio of $Sa(\bar{\omega},\xi)$ to $Spa(\bar{\omega},5\%)$ than that to $Sa(\bar{\omega},5\%)$. Thus, the DMF*a* can be expressed as

$$\mathrm{DMF}a(\bar{\omega},\xi)=\frac{Sa(\bar{\omega},\xi)}{Spa(\bar{\omega},5\%)}=\sqrt{\frac{\int_{0}^{\infty}|Ya(\omega)Ha(\omega,\bar{\omega},\xi)|^{2}d\omega}{\int_{0}^{\infty}|Ya(\omega)Hpa(\omega,\bar{\omega},5\%)|^{2}d\omega}}\cdot\frac{\overline{pf}_{\xi}\sqrt{D_{rms,5\%}}}{\overline{pf}_{5\%}\sqrt{D_{rms,\xi}}} \tag{14}$$

where $D_{rms,5\%}$ and $\overline{pf}_{5\%}$ denote the oscillator-response duration and expected value of the peak factor corresponding to a damping ratio of 5%, respectively. Equation (14) gives an analytical expression for the DMF*a*. As this expression includes various seismological parameters, it allows exploration of the effects of all these parameters on the DMF*a*. It should be noted that Equation (14) is developed to systematically investigate the seismological effects on DMF*a* and theoretically clarify the essential factor governing the seismological effects, and thus, find an appropriate factor that is available from seismic codes to reflect the seismological effects; Equation (14) is not developed for direct implementation in the practical seismic design to calculate the DMF*a*.

Many models for the peak factor have been developed and reported in literatures (Cartwright and Longuet-Higgins1956, Davenport Davenport 1964; Vanmarcke 1975). Wang and Rathje (2016) found that the Vanmarcke model (1975) can give the best estimations of the peak factor among these models. The cumulative distribution function of the peak factor, *pf*, provided by Vanmarcke (1975) is expressed as

$$P(pf<r)=\left[1-e^{(-r^{2}/2)}\right]\times\exp\left[-2f_{z}\exp\left(-r^{2}/2\right)D_{gm}\frac{\left(1-e^{-\delta^{1.2}r\sqrt{\pi/2}}\right)}{\left(1-e^{r^{2}/2}\right)}\right] \tag{15}$$

where, D_{gm} is the ground-motion duration, and δ is a bandwidth factor determined by the spectral moments of FAS and expressed as

$$\delta = \sqrt{1 - \frac{m_1^2}{m_0 m_2}} \tag{16}$$

Here, m_0, m_1, and m_2 are the zeroth-, first-, and second-order spectral moments of the FAS, respectively. The n-th order spectral moment of the FAS, m_n, is defined as

$$m_n = \frac{1}{\pi}\int_0^\infty \omega^n |Ya(\omega)|^2 d\omega \tag{17}$$

In Equation (15), f_z is the rate of zero crossing, which is defined as:

$$f_z = \frac{1}{2\pi}\sqrt{\frac{m_2}{m_0}} \tag{18}$$

The duration of the oscillator response, $D_{rms,\xi}$, in Equation (14) can be related to the ground-motion duration D_{gm}. Boore and Joyner (1984) and Liu and Pezeshk (1999) developed simple formulae to calculate the oscillator-response duration, $D_{rms,\xi}$, from D_{gm}. Boore and Thompson (2012) and then developed a more accurate formula for $D_{rms,\xi}$ as

$$D_{rms,\xi}/D_{gm} = \left[c_{e1} + c_{e2}\frac{1-\eta^{c_{e3}}}{1+\eta^{c_{e3}}}\right]\left[1 + \frac{c_{e4}}{2\pi\xi}\left(\frac{\eta}{1+c_{e5}\eta^{c_{e6}}}\right)^{c_{e7}}\right] \tag{19}$$

Here, $\eta = T_0/D_{gm}$, and c_{e1}–c_{e7} are coefficients that depend on the moment magnitude M and distance R, as noted in Boore and Thompson (2012). The c_e coefficients in Boore and Thompson (2012) were derived using the peak-factor model of Cartwright and Longuet-Higgins (1956). Boore and Thompson (2015) further updated the c_e coefficients using the peak-factor model of Vanmarcke (1975), which are adopted in this paper. In addition, the ground-motion duration D_{gm} that equals a sum of the source and path durations, is estimated based on the model of Boore and Thompson (2014, 2015).

4. Verification of the Analytical Approach

To validate the proposed approach, the calculated DMF*a* results were compared with those obtained from the traditional time-series analysis. A wide range of structural parameters, i.e., structural period T_0 (0.01–10 s) and damping ratio ξ (10–50%), and main seismological parameters, including the moment magnitude M (4–8) and distance R (20–200.01 km), were considered for the calculations. The time series for the analysis was generated from the FAS using the Stochastic Method SIMulation (Boore 2005) program using stochastic simulations (Boore 1983). For each FAS, a suite of 100 time series signals was generated, and the simulated time series matched the FAS on average. Then, the values of the DMF*a* for all the generated time series were calculated using the direct-integration method by Nigam and Jennings (1969). For each FAS, the 100 corresponding DMF*a* results for the same damping level were averaged and compared with those obtained using the proposed approach. Some of these representative comparisons are shown in Fig. 1–3; the favorable agreement in these figures thus validates the proposed approach. Although when the oscillator period is shorter than about 0.03s, the accuracy of the proposed approach deteriorates; such short periods are generally seldom of interest in earthquake engineering.

The DMF*a* trends with variations in the structural and seismological parameters are also investigated. Figure 1 indicates that the DMF*a* is nearly equal to unity at an oscillator period of 0.01 s and decreases to the minimum value (smaller than unity) with increasing oscillator periods. Then, the DMF*a* increases with increasing oscillator periods, and the values may be considerably larger than unity at very long oscillator periods. The decrease and increase rates at short and long oscillator periods are dependent on the damping ratio. Both rates increase with an increase in the damping ratio. In addition, the DMF*a* decreases at short oscillator periods but increases at long oscillator periods with

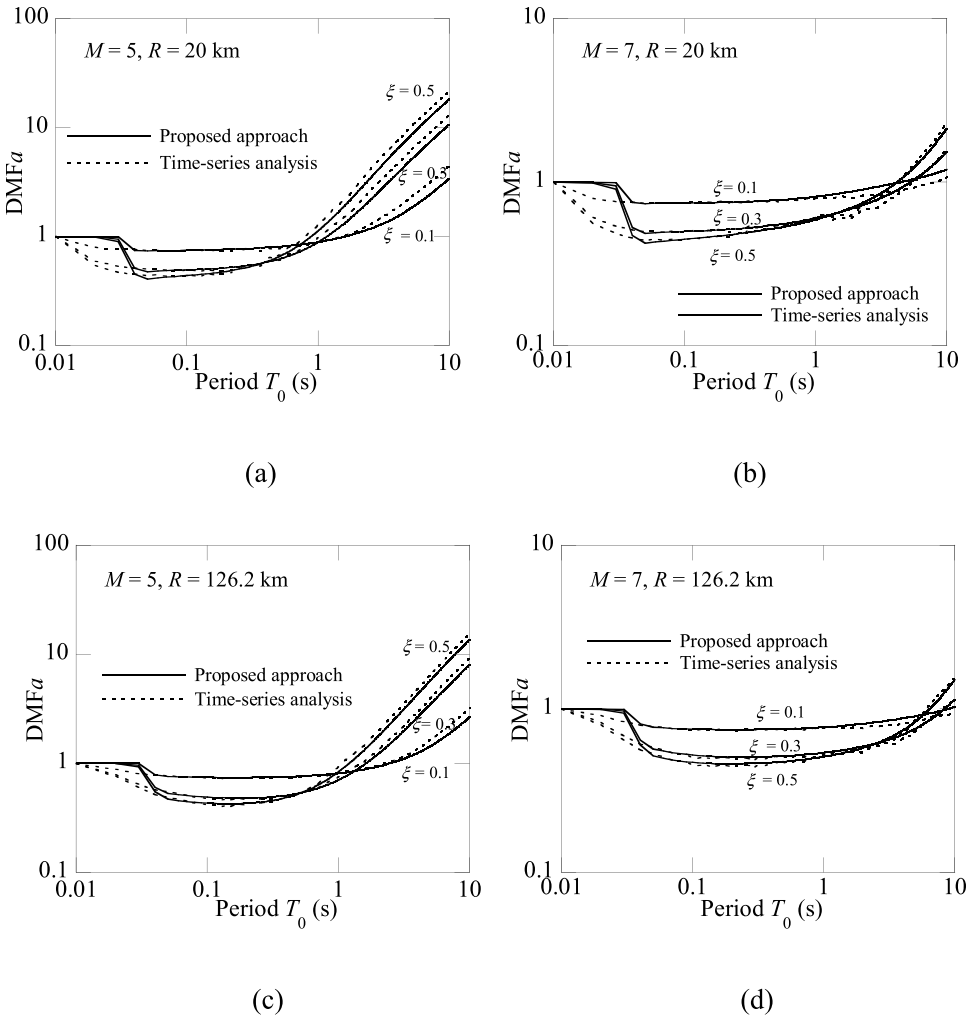

Figure 1. Variation of DMF*a* with damping ratio for moment magnitudes and distances of (a) $M = 5$ and $R = 20$ km, (b) $M = 7$ and $R = 20$ km, (c) $M = 5$ and $R = 126.2$ km, and (d) $M = 7$ and $R = 126.2$ km, respectively.

an increase in damping ratio. The decrease and increase rates at short and long periods corresponding to the damping ratio are dependent on the oscillator period. At long oscillator periods, the DMF*a* increases faster with an increase in the oscillator period.

From Figs. 2 and 3, the DMF*a* trends with variation of seismological parameters can be clarified. Figure 2 indicates that the DMF*a* is dramatically affected by the moment magnitude at long oscillator periods but is essentially independent at short oscillator periods. It is evident from Fig. 2 that the DMF*a* decreases and becomes less dependent on the oscillator period with an increase in moment magnitudes at long oscillator periods. Figure 3 indicates that the behavior of the DMF*a* with variation of the distance R is typically consistent with that of variation of the moment magnitude, but with a much smaller variation degree.

These observed DMF*a* trends with variations in the structural and seismological parameters are consistent with those observed from statistical analyses of real seismic records (Hao et al. 2011; Lin and Chang 2003, 2004; Zhao et al. 2019). The consistency of these observations provides additional verification for the proposed approach for DMF*a*.

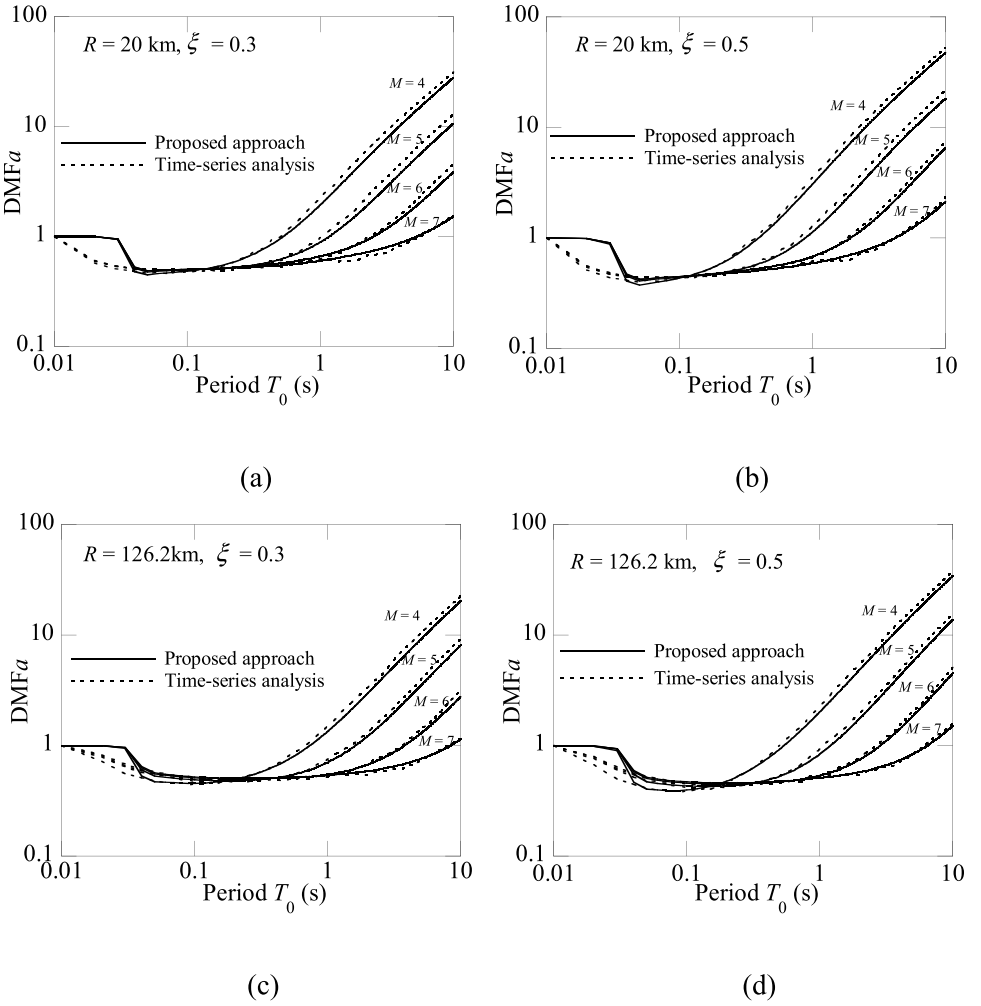

Figure 2. Influence of the moment magnitude on DMF*a* for distances and damping ratios of (a) $R = 20$ km and $\xi = 0.3$, (b) $R = 20$ km and $\xi = 0.5$, (c) $R = 126.2$ km and $\xi = 0.3$, and (d) $R = 126.2$ km and $\xi = 0.5$, respectively.

5. Factor Reflecting the Seismological Effects

To find an appropriate factor that is available from seismic codes to reflect the seismological effects on DMF*a*, the key factor governing the seismological effects is investigated using the proposed approach. For this purpose, the expression for DMF*a*, i.e., Equation (14), is decomposed into three terms. The first term is controlled by the oscillator-response FAS, the second term is controlled by the oscillator-response peak factors, and the third term is controlled by the oscillator-response durations. The results of each of these terms for the cases in Fig. 2 are shown in Fig. 4–6 as representatives showing their contributions to the DMF*a*. It is evident from Figs. 2 and 4 that the DMF*a* is very similar in its first term, and all the characteristics, such as trends with variations in the structural and seismological parameters, are captured adequately in the first term. In addition, Figs. 5 and 6 indicate that the values of the second and third terms are very close to unity compared with those of the first term. All these results indicate that the DMF*a* is dominated by the first term.

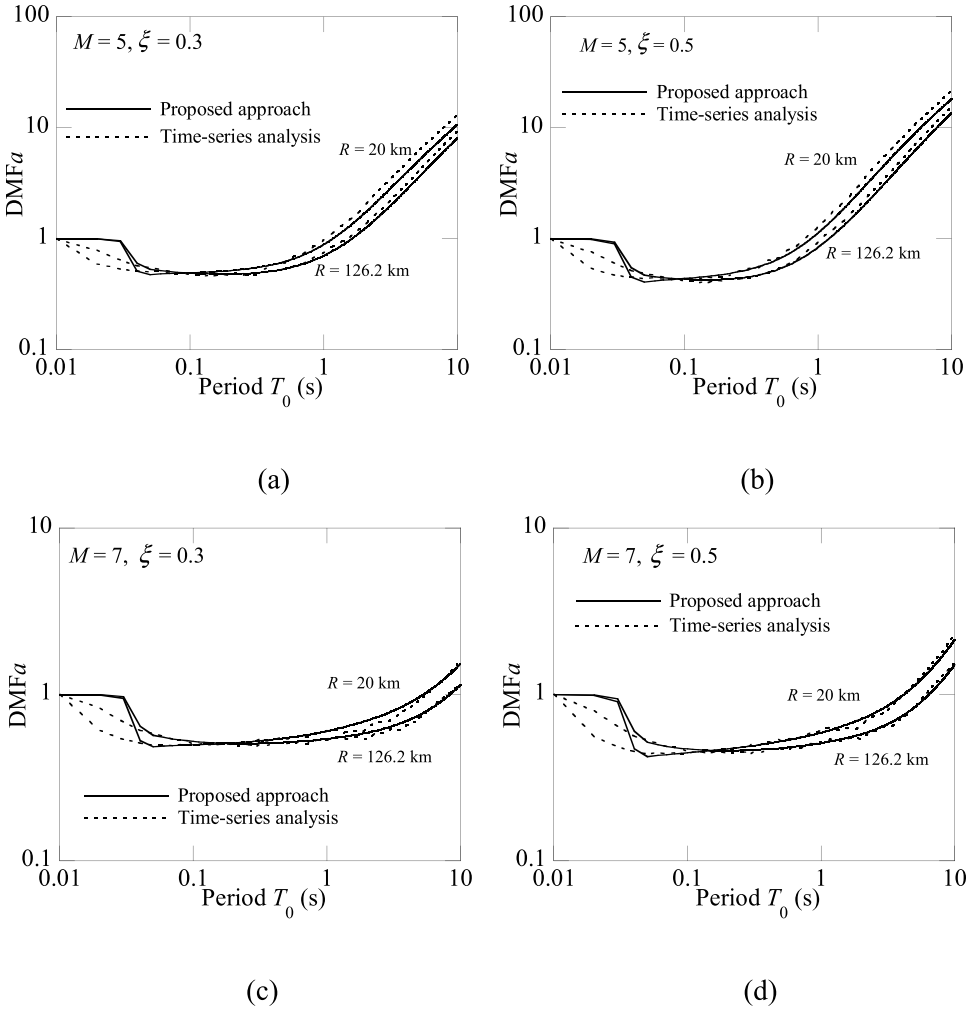

Figure 3. Influence of distance on DMFa for moment magnitudes and damping ratios of (a) $M = 5$ and $\xi = 0.3$, (b) $M = 5$ and $\xi = 0.5$, (c) $M = 7$ and $\xi = 0.3$, and (d) $M = 7$ and $\xi = 0.5$, respectively.

It is evident from Equation (14) that all the seismological parameters including site conditions affect the first term by changing the FAS of the ground motion, $Ya(\omega)$, although only results with respect to moment magnitude and distance are presented. Because the oscillator transfer functions, i.e., $Hpa(\omega, \bar{\omega}, \xi)$ and $Ha(\omega, \bar{\omega}, \xi)$, in the first term are independent of the seismological parameters. In addition, as the first term is expressed in the form of a ratio related to the ground-motion FAS, it should be the relative value of the FAS rather than its absolute value that affects the first term. This can be easily understood by scaling the ground-motion FAS by a constant value. As the constant value exists for the numerator and denominator and then disappears, the first term will not be changed. Moreover, the relative value or shape of the FAS physically represents the frequency content of the ground motions. Therefore, the key factor governing the seismological effects is the frequency content of the ground motion, and all the seismological parameters, including the moment magnitude, distance, and site conditions, affect the DMFa mainly by changing the ground-motion frequency content.

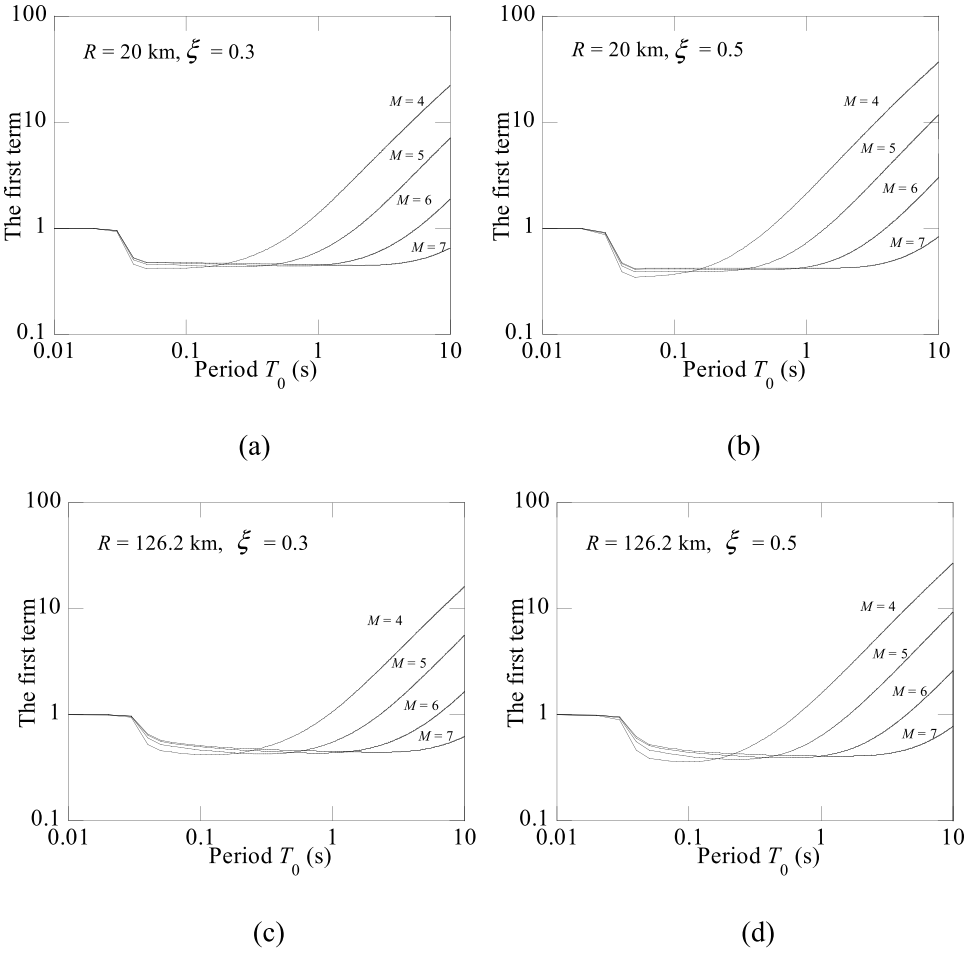

Figure 4. Values of the first term of the DMF*a* for distances and damping ratios of (a) $R = 20$ km and $\xi = 0.3$, (b) $R = 20$ km and $\xi = 0.5$, (c) $R = 126.2$ km and $\xi = 0.3$, and (d) $R = 126.2$ km and $\xi = 0.5$, respectively.

The aforementioned findings facilitate the determination of a single factor that can represent the ground-motion frequency content to reflect the seismological effects on the DMF*a*. Boore (2003) introduced a bandwidth factor ζ, which can reflect the ground-motion frequency content

$$\zeta = \frac{m_2}{\sqrt{m_0 m_4}} \tag{20}$$

However, the bandwidth factor ζ is also not defined as a part of the seismic design actions in existing seismic codes. To solve this problem, the bandwidth factor ζ should be related to the parameters available in seismic codes. Equation (20) indicates that the bandwidth factor ζ is a function of the spectral moments of the FAS, and the RVT states that the square of the zeroth-order spectral moment of the FAS is proportional to the peak ground motion (PGM) (Boore 1983, 2003) given as

$$PGM = \sqrt{m_0} \times \overline{pf} / \sqrt{D_{gm}} \tag{21}$$

Therefore, the square of the zeroth-order spectral moment of the displacement FAS $Yd(\omega)$, is proportional to the peak ground displacement (PGD), which can be expressed as

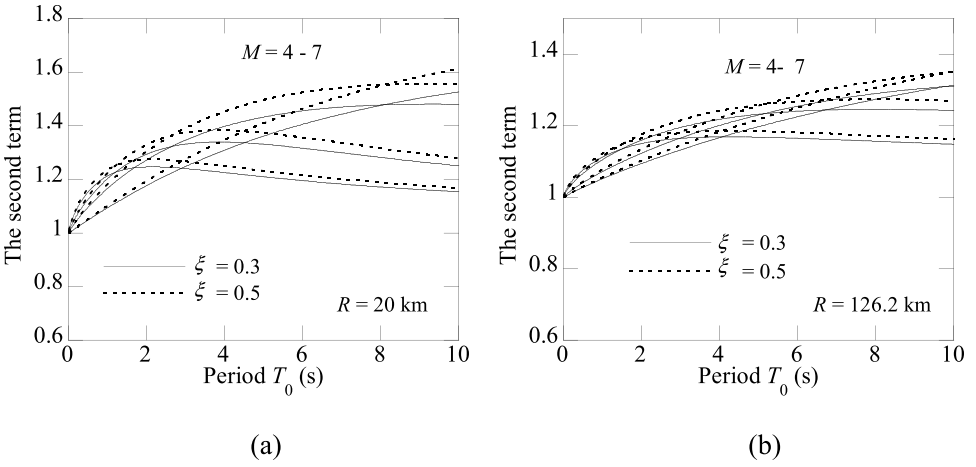

Figure 5. Values of the second term of the DMF*a* for distances and damping ratios of (a) R = 20 km, ξ = 0.3 and 0.5 and (b) R = 126.2 km, ξ = 0.3 and 0.5.

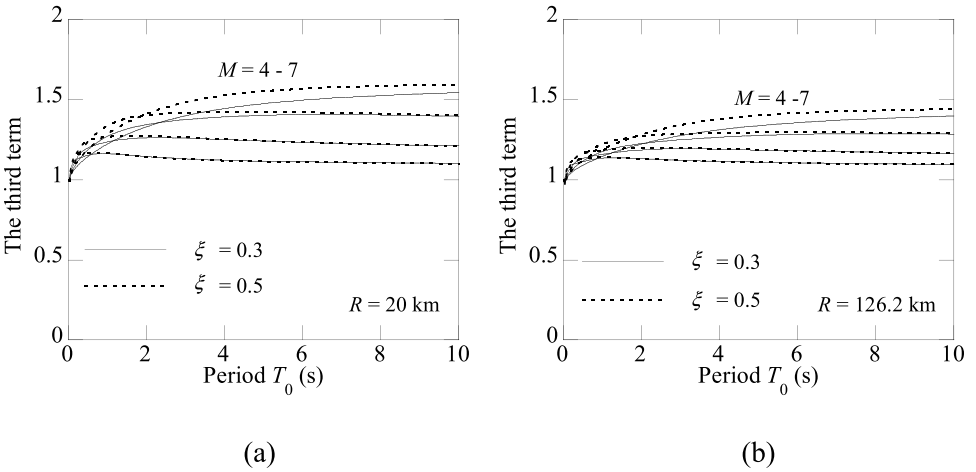

Figure 6. Values of the third term of the DMF*a* for distances and damping ratios of (a) R = 20 km, ξ = 0.3 and 0.5 and (b) R = 126.2 km, ξ = 0.3 and 0.5.

$$\sqrt{m_0} = \sqrt{\int_0^\infty |Yd(\omega)|^2 d\omega} \propto \mathrm{PGD} \tag{22}$$

In addition, because the FAS of the velocity, $Yv(\omega)$, is related to that of the displacement as $Yv(\omega) = \omega Yd(\omega)$, the square of the second-order moment of the displacement FAS equals that of the zeroth-order moment of the velocity FAS, and is thus proportional to the peak ground velocity (PGV), which can be expressed as

$$\sqrt{m_2} = \sqrt{\int_0^\infty \omega^2 |Yd(\omega)|^2 d\omega} = \sqrt{\int_0^\infty |Yv(\omega)|^2 d\omega} \propto \mathrm{PGV} \tag{23}$$

Similarly, because the FAS of the acceleration can be obtained from that of the displacement by $Ya(\omega) = \omega^2 Yd(\omega)$, the square of the fourth-order moment of the displacement FAS equals that of the zeroth-order moment of the acceleration FAS, and is thus proportional to the peak ground acceleration (PGA), which can be expressed as

$$\sqrt{m_4} = \sqrt{\int_0^\infty \omega^4 |Yd(\omega)|^2 d\omega} = \sqrt{\int_0^\infty |Ya(\omega)|^2 d\omega} \propto \mathrm{PGA} \tag{24}$$

Substituting Equations. (22)–(24) into Equation (20), ζ can be expressed as

$$\zeta = \frac{\mathrm{PGV}^2}{\mathrm{PGD} \times \mathrm{PGA}} \tag{25}$$

Here, Equation (25) implicitly assumes that the peak factor and duration that link the zeroth-order spectral moment to the peak value are similar for the ground acceleration, velocity, and displacement.

Since PGV and PGD are also generally not provided in seismic codes, it is desirable to link them to the design spectrum. Here, it is assumed that PGV and PGD are related to the pseudo velocity spectrum *Spv* and displacement spectrum *Sd* at a specific period T_S, respectively. Furthermore, *Spv* and *Sd* can be converted to the pseudo acceleration spectrum *Spa* by $Spv = Spa/\omega_0$ and $Sd = Spa/\omega_0^2$. Therefore, a new bandwidth factor ζ_b is introduced as

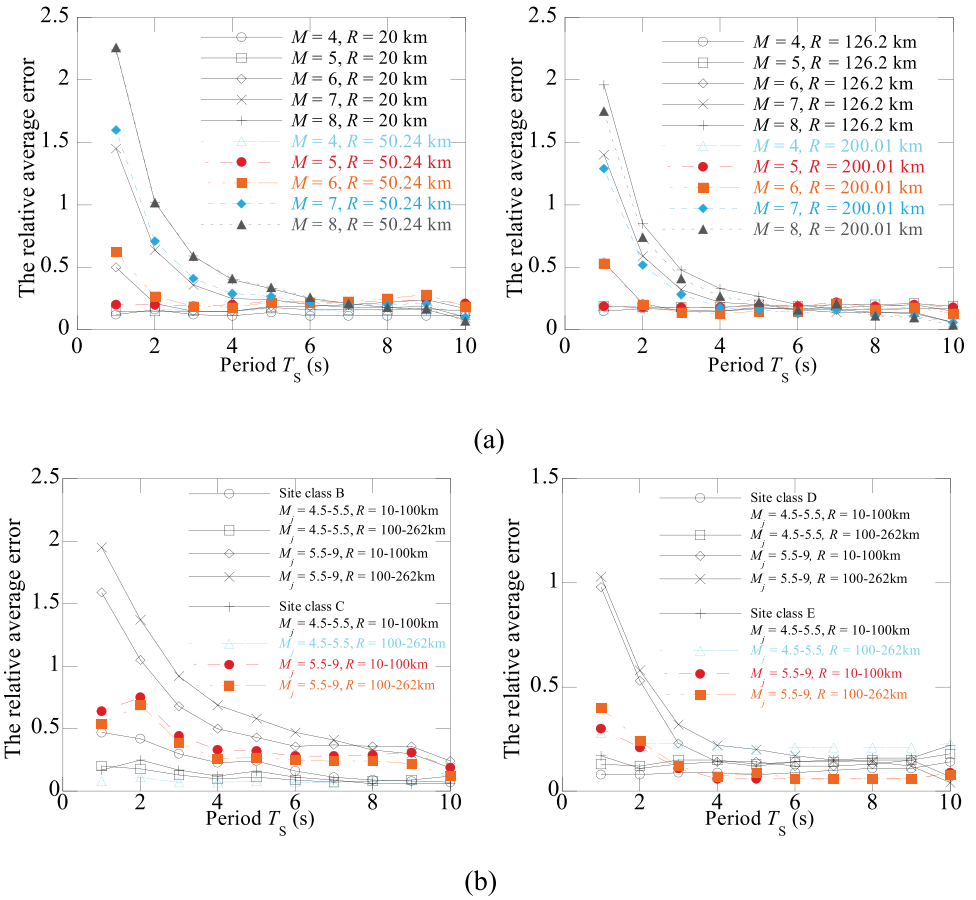

Figure 7. The relative average error of DMF*a* at 0.01 to 10 s compared with results of (a) the time-series analysis in Section 4 and (b) real ground motion records.

$$\zeta_b = \frac{(Spa(T_S)/\omega_0)^2}{Spa(T_S)/\omega_0^2 \times \mathrm{PGA}} = \frac{Spa(T_S)}{\mathrm{PGA}} \tag{26}$$

Although the values of ζ and ζ_b may be different, they must be closely related to each other. Therefore, the parameter ζ_b should also be able to represent the frequency content of the ground motion, which will be confirmed below.

Then, to find a proper value of T_S, 10 periods (1–10 s with 1-s interval) were attempted to understand using which period ζ_b can better reflect the seismological effects on DMF*a*. The bandwidth factor ζ_b using the 10 periods calculated by Equation (26) was all applied to derive the DMF*a* formulation following the process in Section 6. The relative average error of DMF*a* at 0.01 to 10 s compared with results of the time-series analysis in Section 4 and real seismic records detailed below are shown in Fig. 7. The relative average error decreases with increasing T_S, and it becomes stable from 6 s. Since the longest period of the design spectrum is generally limited (e.g., the longest period is 6 s in GB 50011–2010), a period as short as possible is selected. Therefore, the bandwidth factor is calculated using $\zeta_b = Spa(6\ \mathrm{s})/\mathrm{PGA}$ (or $\zeta_b = Spa(6\ \mathrm{s})/Spa(0\ \mathrm{s})$), in this study.

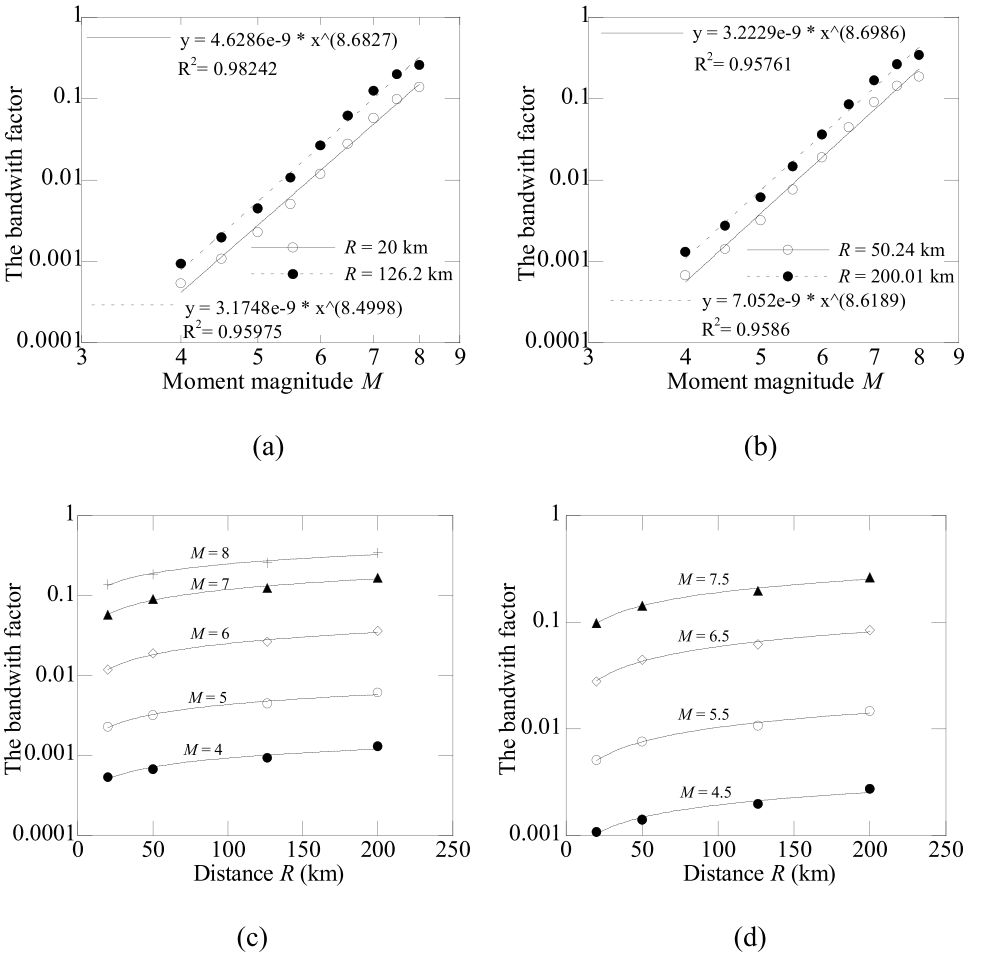

Figure 8. Correlation between the bandwidth factor ζ_b and (a) moment magnitudes for distances of 20 km and 126.2 km, (b) moment magnitudes for distances of 50.24 km and 200.01 km, (c) distances for moment magnitudes of 4, 5, 6, 7, and 8, and (d) distances for moment magnitudes of 4.5, 5.5, 6.5, and 7.5.

Formally, the PGV and PGD in Equation (25) can be estimated from the peaks in the corresponding response spectrum using the equations of Booth (2007). However, the peak of the displacement spectrum is not available in some seismic codes (e.g., Japanese seismic code 2000), since the displacement spectrum converted from *Spa* increases indefinitely with the period. Therefore, this approach is not adopted in this study.

Then, to show the capability of the bandwidth factor to reflect the seismological effects, its correlations with the main seismological parameters are presented in Fig. 8. It is evident from this figure that the bandwidth factor ζ_b is closely related to the seismological parameters and increases with increasing moment magnitudes and distances. R^2 of correlation for all these cases are as large as approximately 0.96. In addition, trends in the DMF*a* with variations of the moment magnitudes and distances are compared with those with variations of the corresponding bandwidth factors in Figs. 9 and 10, respectively. It is found that the trend in the DMF*a* with variation of the bandwidth factor is consistent with the variation of the moment magnitude and distance. The favorable correlations in these figures support the ability of the derived bandwidth factor to reflect the seismological effects.

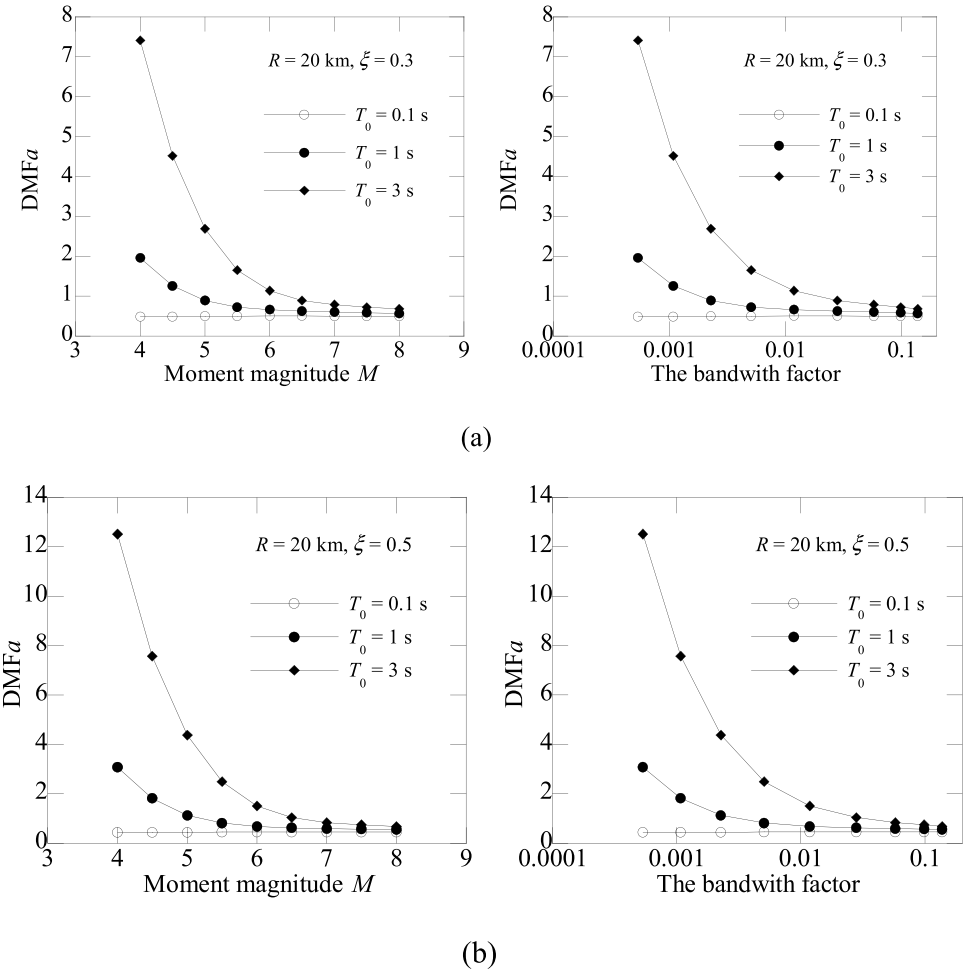

Figure 9. Comparison of trends in the DMF*a* with variations of the moment magnitudes and bandwidth factors for distances and damping ratios of (a) R = 20 km, ξ = 0.3 and (b) R = 20 km, ξ = 0.5.

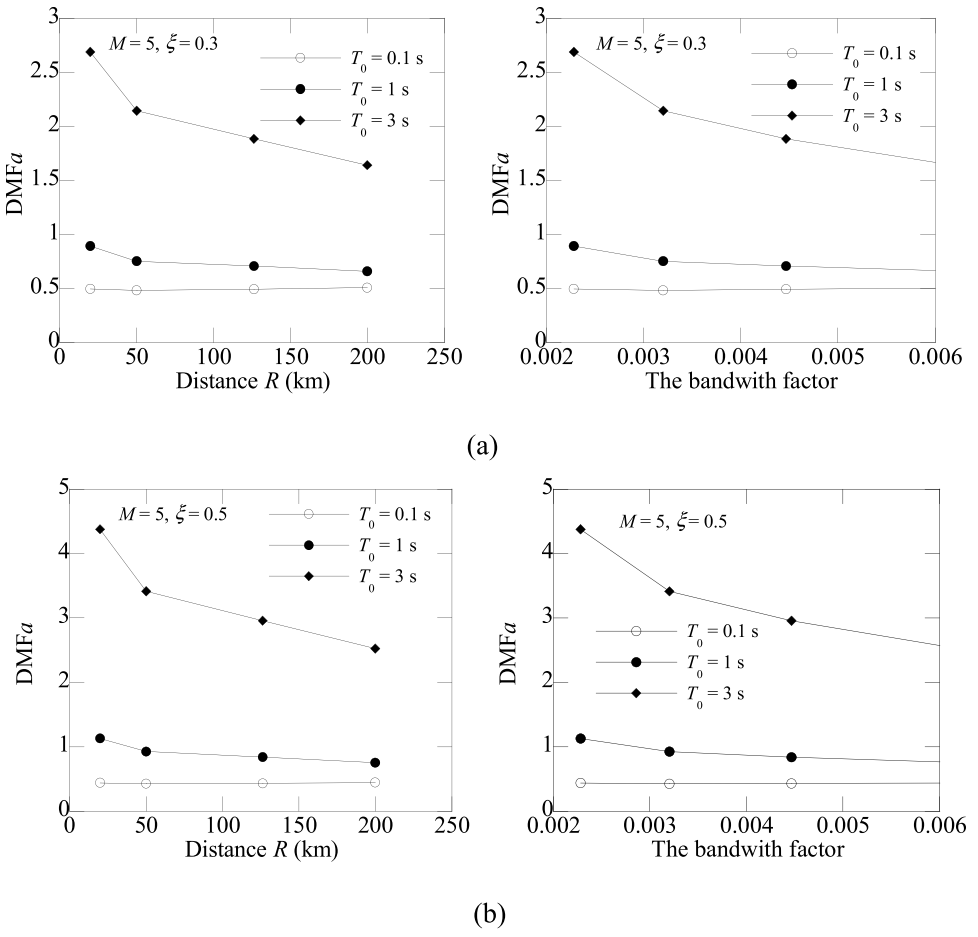

Figure 10. Comparison of trends in the DMFa with variations of distances and bandwidth factors for moment magnitudes and damping ratios of (a) M = 5 km, ξ = 0.3 and (b) M = 5, ξ = 0.5.

To further confirm the capability of the bandwidth factor to reflect the seismological effects, its correlations with magnitude, distance, and site conditions are analyzed based on real seismic records. For this purpose, 16660 seismic ground-motion records with a wide range of magnitude (4–9) and rupture distance (10–262 km) are selected from Strong-motion Seismograph Networks (K-NET, KiK-net) of Japan (NIED 1995). The magnitude M_j adopted in the K-NET and KiK-net is the Japan Meteorological Agency magnitude. The peak ground motion acceleration of each record is larger than 20 gal; this is set to guarantee a sufficient signal-to-noise ratio. These seismic ground motions were recorded at 338 stations in Japan. The average shear-wave velocity in the upper 30 m (V_{30}) of the stations varies from 106 to 1437 m/s, which cover the four site classes (B, C, D, and E) defined in the NEHRP (2000). Based on the criterion adopted by Hatzigeorgiou (2010), 98% of these records are far-field (R > 20 km), no near-fault (< 10 km) motions are included, and 2% of the records are in between. Then, representative results of the bandwidth factor ζ_b versus magnitude, site conditions, and rupture distance are presented in Fig. 11. It is evident from Fig. 11 a and b that the bandwidth factor ζ_b is closely related to the magnitude. Similarly, Fig. 11 c and d show that the average value of the bandwidth factor ζ_b in each group classified based on magnitude and distance, is also closely related to site conditions. Poor correlation between the bandwidth factor ζ_b and the rupture distance is observed (Fig. 11 e and f). This is because

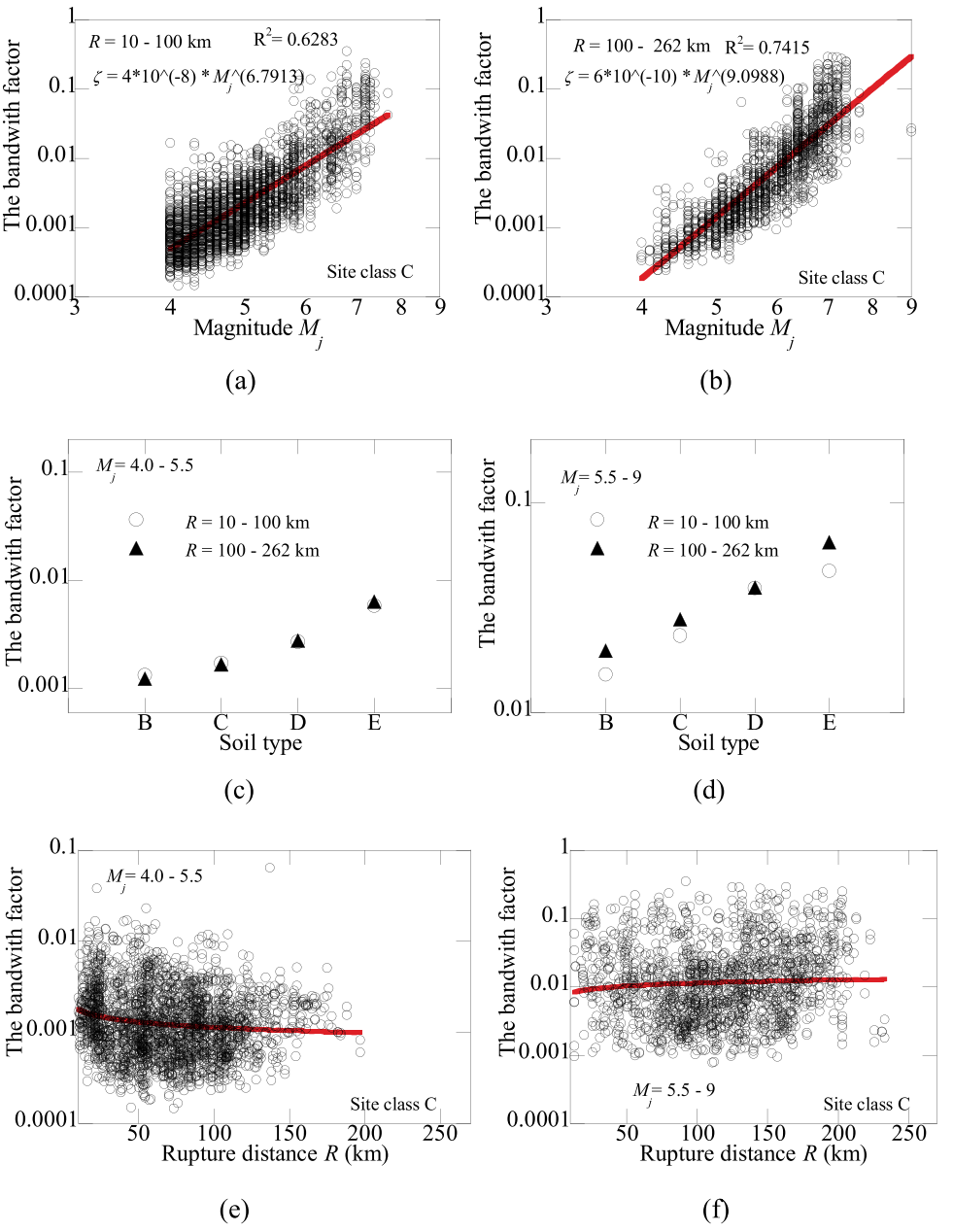

Figure 11. Correlation between the bandwidth factor ζ_b and (a) magnitudes M_j for distances from 10 to 100 km, (b) magnitudes M_j for distances from 100 to 262 km, (c) site conditions for magnitudes M_j from 4.0 to 5.5, (d) site conditions for magnitudes M_j from 5.5 to 9, (e) distances for magnitudes M_j from 4.0 to 5.5, and (f) distances R for magnitudes M_j from 5.5 to 9, based on real seismic records.

a magnitude range instead of a particular value is used for the investigation, and the effect of magnitude on ζ_b is much more significant than the effect of the rupture distance on ζ_b (Fig. 8). In general, the derived factor can reflect the main seismological effects.

Craifaleanu (2011) has tested other definitions of the frequency content measures and sustained the possible use of velocity spectrum-related parameters in describing the frequency content of narrow frequency band motions. The abilities of the four velocity-spectrum-related parameters, i.e., the predominant period T_{gSV}, modified spectral characteristic period T^*_{mean}, modified central period

T^*_{cen}, and modified shape factor q^*, in reflecting the seismological effects on DMFa are also tested. Based on the results in Section 4, it is found that (not shown here) the four parameters are also closely related to magnitude and distance. Nevertheless, when they were applied to derive the DMFa formulation following the process in Section 6, the DMFa results using the derived bandwidth factor ζ_b are more stable and agree better with those of real seismic records than the velocity-spectrum-related parameters. Moreover, the bandwidth factor ζ_b can be more easily obtained from the acceleration spectrum specified in seismic codes.

6. Practical DMFa Formulation

6.1. Proposal of the DMFa Formulation

According to the above discussions, a practical DMFa formulation considering the seismological effects is presented in this section. A large number of function forms were tested to fit the results of the DMFa in Section 4, by considering a balance between simplicity and accuracy. A piecewise linear function is found to adequately capture the main characteristics of the DMFa, and is expressed as

$$\mathrm{DMF}a = \begin{cases} 1 + \frac{\mathrm{DMF}a(T_{\min})-1}{T_{\min}} T_0 & T_0 \le T_{\min} \\ \mathrm{DMF}a(T_{\min}) + k_0(T_0 - T_{\min}) & T_0 > T_{\min} \end{cases} \tag{27}$$

where, DMF$a(T_{\min})$ is the minimum DMFa value; $T_{\min}$ is the period corresponding to DMF$a(T_{\min})$, and k_0 is a parameter responsible for controlling the increase rate of DMFa with the period at $T_0 > T_{\min}$. Equation (27) is totally controlled by the three factors, i.e., $T_{\min}$, DMF$a(T_{\min})$, and k_0.

As the DMFa is essentially unaffected by the seismological parameters at $T_0 \le T_{\min}$ (Figs. 2 and 3), Equation (27) is independent of these parameters for $T_0 \le T_{\min}$. Therefore, the DMF$a(T_{\min})$ is a function of only the damping ratio ξ and is expressed as

$$DMFa(T_{\min}) = 0.33/\xi^{0.34} \tag{28}$$

Figure 12 shows the accuracy of Equation (28).

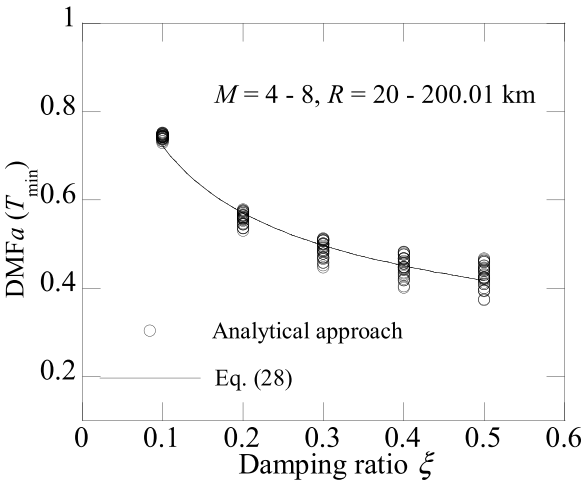

Figure 12. Variation of DMF$a(T_{\min})$ with the damping ratio ξ.

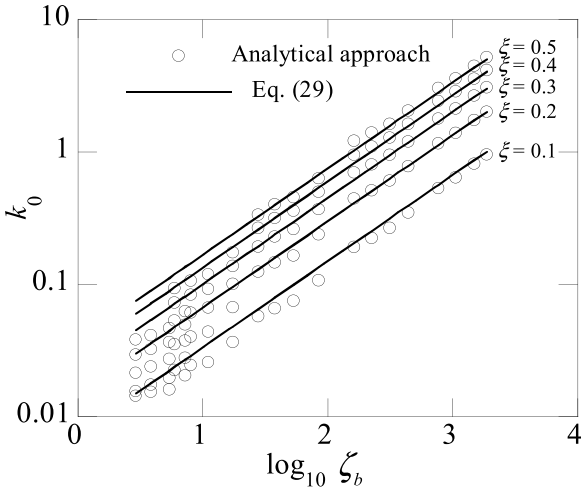

Figure 13. Variation of the parameter k_0 with the bandwidth factor ζ_b.

The DMF*a* is significantly affected by the seismological parameters for $T_0 > T_{\min}$. Therefore, Equation (27) incorporates the seismological effects for $T_0 > T_{\min}$. Section 5 indicates that the bandwidth parameter ζ_b can properly reflect the seismological effects. In addition, the seismological parameters influence the DMF*a* mainly by changing the increase rate with respect to the period for $T_0 > T_{\min}$, which is reflected by k_0 in Equation (27). Therefore, k_0 is expressed as a function of ζ_b and regressed as

$$k_0 = 0.075\xi e^{-1.5\log_{10}\zeta_b} \tag{29}$$

Figure 13 shows the accuracy of Equation (29).

In addition, it is found from the results in Section 4 that $T_{\min}$ varies slightly with the seismological parameters and almost do not change with the damping ratio. Therefore, $T_{\min}$ is considered to be a function of ζ_b, and a simple equation is regressed as

$$T_{\min} = 0.7\zeta_b + 0.1 \tag{30}$$

Although the $T_{\min}$ scattering seems large in Fig. 14, the DMF*a* accuracy is found to be not sensitive to that of $T_{\min}$.

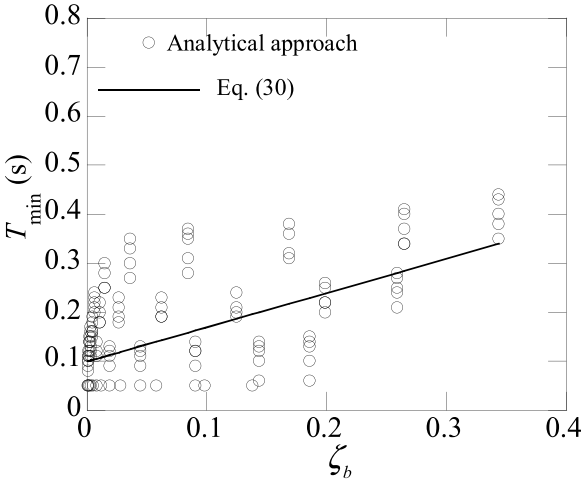

Figure 14. Variation of the period $T_{\min}$ with the bandwidth factor ζ_b.

Then the DMF*a* results by Equation (27) are compared with those calculated using the analytical approach (Equation (14)) and time-series analysis introduced in Section 4. Some representative comparisons are presented in Fig. 15. The DMF*a* results of Equation (27) are typically consistent with those obtained by the analytical approach and time-series analysis. Although the error at short periods (< 1 s) seems large in logarithmic coordinates, the relative average error at periods from 0.01 to 10 s is limited to approximately 20%.

6.2. Comparison with Results of Seismic Records and Existing Formulations

The DMF*a* results by Equation (27) are further compared with those of real seismic records used in Section 5 as well as existing formulations in literatures (Hatzigeorgiou 2010; Lin and Chang 2004). The seismic records in each site class are divided into four groups according to

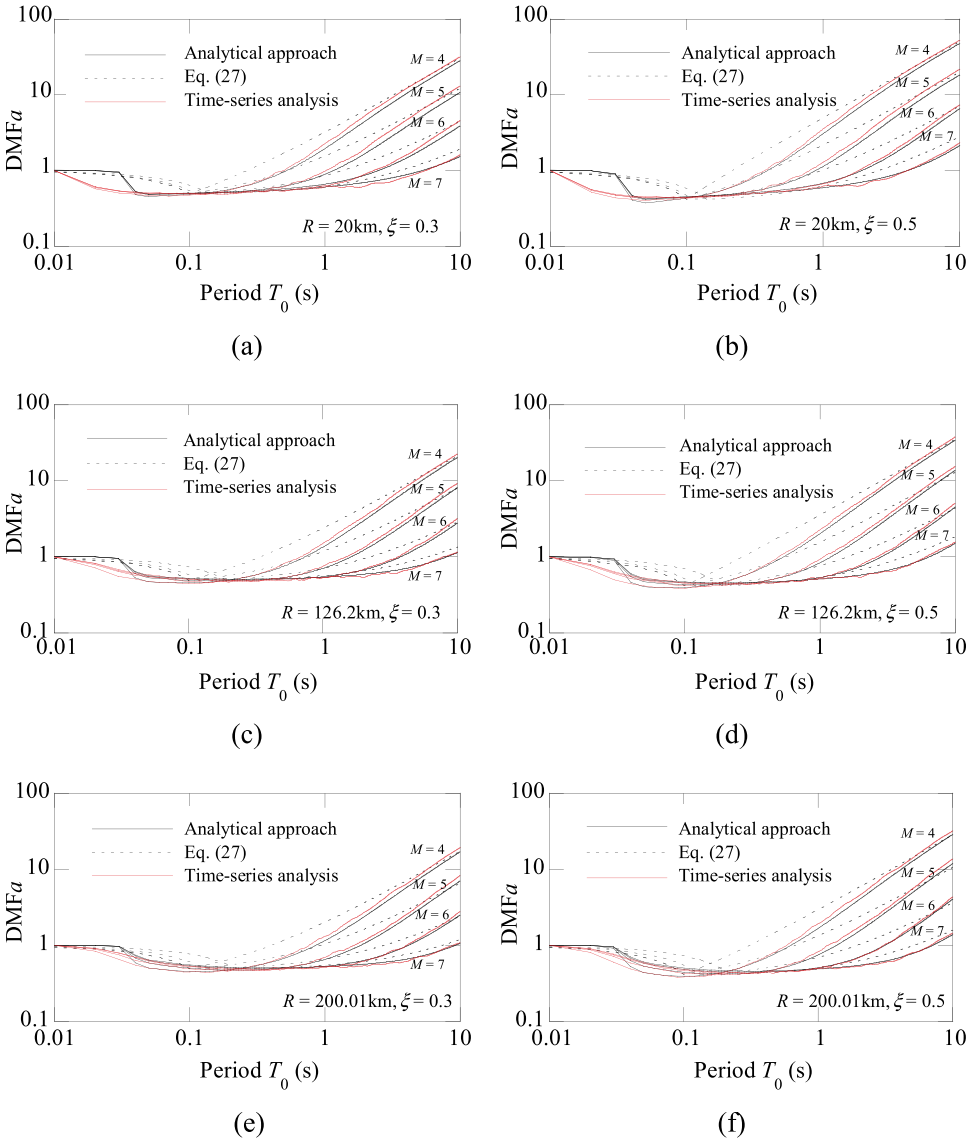

Figure 15. Comparison of the DMF*a* results by Eq. (27), analytical approach (Eq. (14)), and time-series analysis for distances and damping ratios of (a) R = 20 km and ξ = 0.3, (b) R = 20 km and ξ = 0.5, (c) R = 126.2 km and ξ = 0.3, (d) R = 126.2 km and ξ = 0.5, (e) R = 200.01 km and ξ = 0.3, (f) R = 200.01 km and ξ = 0.5, respectively.

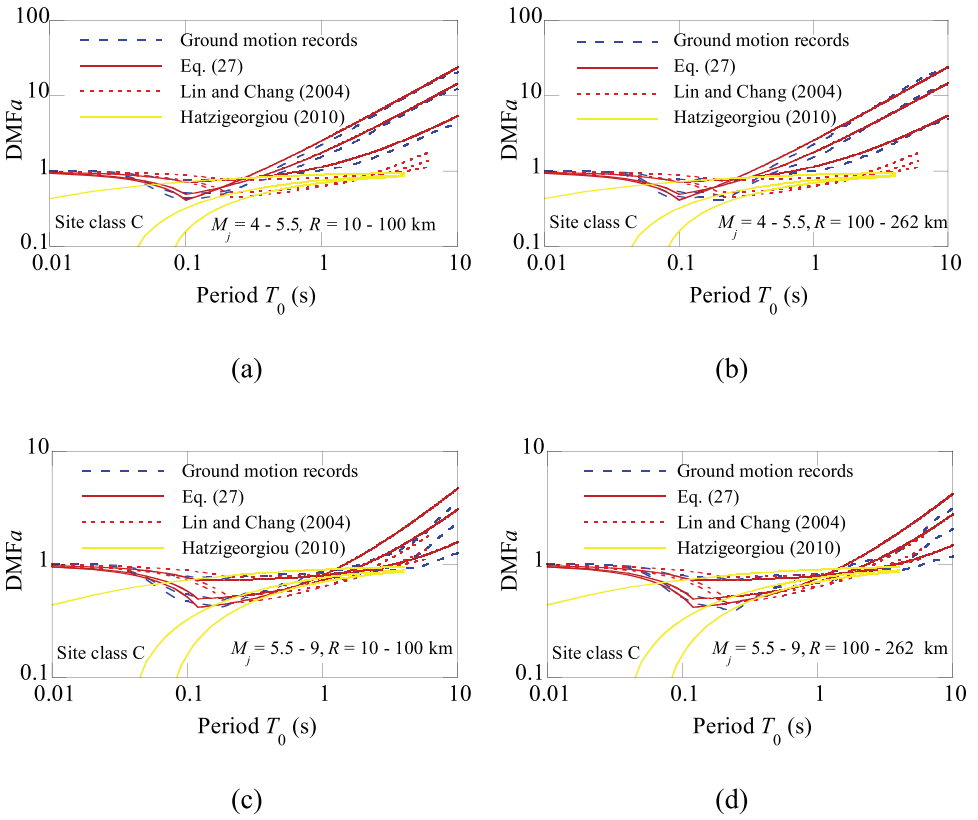

Figure 16. Comparison of the DMF*a* results by Eq. (27), statistical analysis of seismic records in site class C, and existing formulations in the literature for magnitudes and distances of (a) M_j = 4–5.5, R = 10–100 km, (b) M_j = 4–5.5, R = 100–262 km, (c) M_j = 5.5–9, R = 10–100 km, (d) M_j = 5.5–9, R = 100–262 km, respectively.

magnitude and distance as shown in Figs. 16 and 17, considering a balance of records number. The average DMF*a* results in each group are compared with those calculated by Equation (27) and formulations of Lin and Chang (2004) and Hatzigeorgiou (2010). As similar trends are observed in the four site classes, only results of site classes C and D are shown as representatives in Figs. 16 and 17, respectively. It is evident from both figures that, results by Equation (27) agree well with those of real seismic records and better than those by formulations of Lin and Chang (2004) and Hatzigeorgiou (2010). Although the error of Equation (27) increases for large magnitude, the relative average error at periods from 0.01 to 10 s is limited to approximately 20%.

6.3. Application of the DMFa Formulation

This section presents the applicability of Equation (27) in calculating the DMF*a* in the practical seismic design. Using the 5%-damped design spectra specified in Eurocode 8 (2004) and Japanese seismic code (2000), the DMF*a* and acceleration spectra for two damping levels (10% and 30%) are calculated. As the period of the design spectra in Eurocode 8 (2004) is limited to 4 s, *Spa* (6 s) used for the calculation of the bandwidth factor ζ_b is obtained by

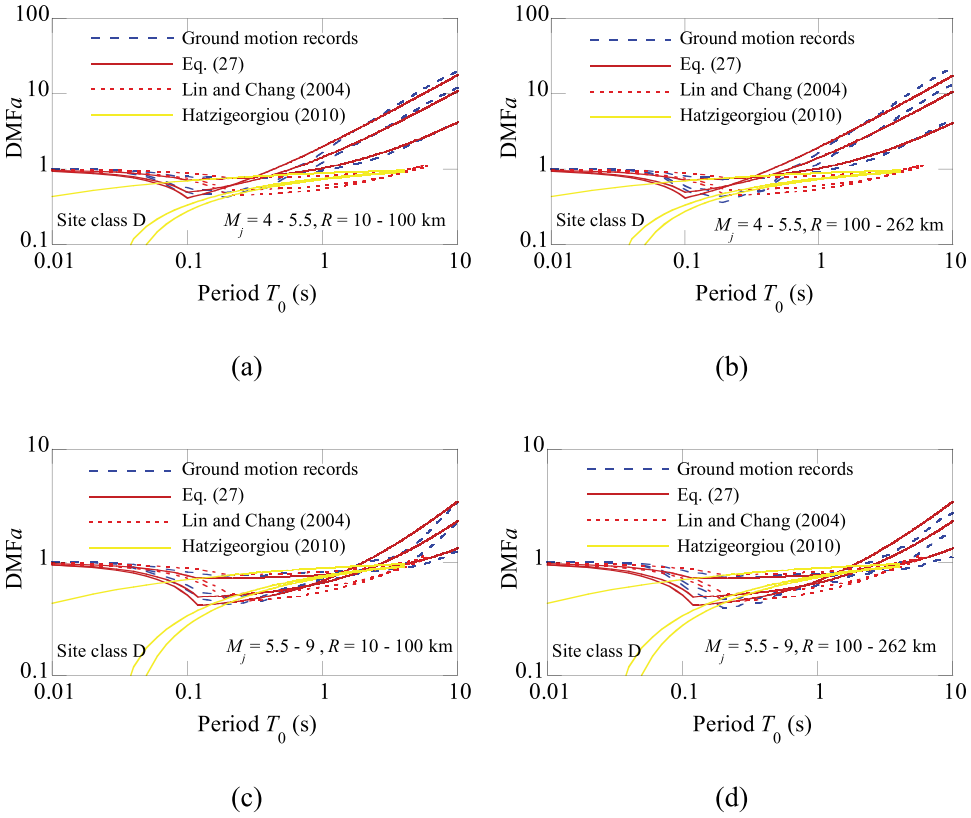

Figure 17. Comparison of the DMF*a* results by Eq. (27), statistical analysis of seismic records in site class D, and existing formulations in the literature for magnitudes and distances of (a) M_j = 4–5.5, R = 10–100 km, (b) M_j = 4–5.5, R = 100–262 km, (c) M_j = 5.5–9, R = 10–100 km, (d) M_j = 5.5–9, R = 100–262 km, respectively.

extending the spectra based on the expression for long periods. Hence, parameters needed for Equation (27) are all available; the DMF*a* and acceleration spectra can be readily obtained and shown in Fig. 18. The obtained acceleration spectra are all normalized by PGA.

As can be seen from Fig. 18, the DMF*a* varies with the spectral type and site class owing to the variations in the frequency content. The spectra of Type 1 and Type 2 in Eurocode 8 (2004) are applied for seismic designs considering large and small surface-wave magnitude M_s (i.e., $M_s > 5.5$ and $M_s \leq 5.5$), respectively. The DMF*a* results are also found to be different for the two seismic codes. It should be noted that the definitions of the soil type are different in the two seismic codes. The DMF*a* results of the Japanese Seismic Design Code (2000) are relatively similar to those of the Type 1 spectra ($M_s > 5.5$) in Eurocode 8 (2004).

7. Conclusions

This study proposes a practical formulation for the damping modification factor of the true acceleration response spectrum (DMF*a*) considering the seismological effects (e.g., magnitude, distance, and site conditions). To this end, an analytical approach was developed based on random vibration theoryto systematically explore the seismological effects on DMF*a*, and clarify the key factor governing the seismological effects. The main findings of this study are summarized as follows:

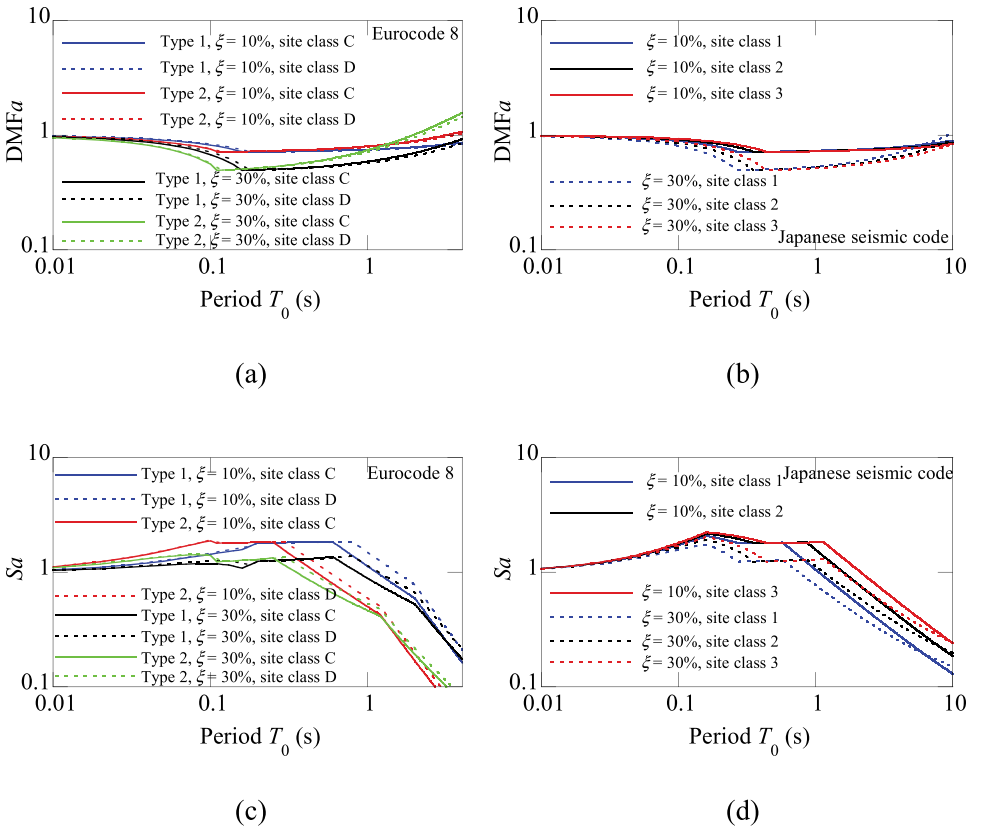

Figure 18. The DMF*a* results by Eq. (27) for design spectra in (a) Eurocode 8 (2004) and (b) Japanese Seismic Design Code (2000), respectively; and corresponding normalized spectral accelerations for spectra in (c) Eurocode 8 (2004) and (d) Japanese Seismic Design Code (2000), respectively.

(1) The developed analytical approach can provide a good estimate of the DMF*a* compared to the results of the time-series analysis and allows systematical exploration of the seismological effects.

(2) The seismological effects on the DMF*a* are governed by the frequency content of the ground motions.

(3) The frequency content of the ground motions can be quantified using a bandwidth factor ζ_b, expressed as the ratio of acceleration spectral values at 6 and 0 s, which can be easily obtained from the design spectra.

(4) The proposed simple DMF*a* formulation incorporating the derived bandwidth factor ζ_b can be easily applied in the practical seismic design and give reasonable estimations of the DMF*a* compared to the results of real seismic records.

Acknowledgments

Funding for this study was provided by the National Natural Science Foundation of China (Grant No. 51738001), which is gratefully acknowledged. The authors are also grateful to Baojian Hang, Zheng Liu, and Jia Deng for aiding in the selection of earthquake data. The authors thank Editor Sinan Akkar and two anonymous reviewers for their perceptive and useful comments, which led to significant improvements in the article.

Disclosure Statement

No potential conflict of interest was reported by the author(s).

Funding

This work was supported by the National Natural Science Foundation of China [51738001].

References

Ashour, S. A. 1987. Elastic seismic response of buildings with supplemental damping. Ph.D. Thesis, Department of Civil Engineering, Michigan University.

Bommer, J. J., and A. S. Elnashai. 1999. Displacement spectra for seismic design. *Journal of Earthquake Engineering* 3: 1–32.

Bommer, J. J., and R. Mendis. 2005. Scaling of spectral displacement ordinates with damping ratios. *Earthquake Engineering & Structural Dynamics* 34: 145–65.

Boore, D. M. [2005] SMSIM—Fortran programs for simulating ground motions from earthquakes: Version 2.3, U.S. Geol. Surv. Open-File Rept. 2005 OFR 96-80-A, Menlo Park, California.

Boore, D. M., and E. M. Thompson. 2012. Empirical improvements for estimating earthquake response spectra with random-vibration theory. *Bulletin of the Seismological Society of America* 102: 761–72.

Boore, D. M., and E. M. Thompson. 2014. Path durations for use in the stochastic-method simulation of ground motions. *Bulletin of the Seismological Society of America* 104: 2541–52.

Boore, D. M., and E. M. Thompson. 2015. Revisions to some parameters used in stochastic-method simulations of ground motion. *Bulletin of the Seismological Society of America* 105: 1029–41.

Boore, D. M., and W. B. Joyner. 1984. A note on the use of random vibration theory to predict peak amplitudes of transient signals. *Bulletin of the Seismological Society of America* 745: 2035–39.

Boore, D. M. 1983. Stochastic simulation of high-frequency ground motions based on seismological models of the radiated spectra. *Bulletin of the Seismological Society of America* 73: 1865–94.

Boore, D. M. 2003. Simulation of ground motion using the stochastic method. *Pure and Applied Geophysics* 60: 635–76.

Booth, E. 2007. The estimation of peak ground-motion parameters from spectral ordinates. *Journal of Earthquake Engineering* 11 (1): 13–32.

Brune, J. 1970. Tectonic stress and the spectra of seismic shear waves from earthquakes. *Journal of Geophysical Research Atmospheres* 75 (26): 4997–5009.

Brune, J. 1971. Correction. *Journal of Geophysical Research* 76 (20): 5002.

Cameron, W. I., and R. U. Green. 2007. Damping correction factors for horizontal ground-motion response spectra. *Bulletin of the Seismological Society of America* 3: 934–60.

Cartwright, D. E., and M. S. Longuet-Hlggms. 1956. The statistical distribution of the maxima of a random function. *Proceedings of the Royal Society of London. Series A, Mathematical and Physical Sciences* 237: 212–23.

Castillo, T., and S. E. Ruiz. 2014. Reduction factors for seismic design spectra for structures with viscous energy dampers. *Journal of Earthquake Engineering* 18 (3): 323–49.

Conde-Conde, J., and A. Benavent-Climent. 2019. Construction of elastic spectra for high damping. *Engineering Structures* 191: 343–57.

Constantinou, M. C., T. T. Soong, and G. F. Dargush. 1998. Passive energy dissipation systems for structural design and retrofit. In *Monograph series*. New York: MCEER, Buffalo 23–26 .

Craifaleanu, I. G. 2011. Investigation of the frequency content of ground motions recorded during strong Vrancea earthquakes, based on deterministic and stochastic indices. *Eighth International Conference on Structural Dynamics*, EURODYN, Leuven, Belgium, July 4-6, paper no. MS16-832 (on CD/ROM).

Davenport, A. G. 1964. Note on the distribution of the largest value of a random function with application to gust loading. *Proceedings of the Institution of Civil Engineers* 28: 187–96.

Electric Power and Research Institute (EPRI). 1993. Guidelines for determining design basis ground motions. Volume 1: Method and guidelines for estimate earthquake ground motion in eastern north America . , Palo Alto, Calif: EPRI. TR-102293.

Eurocode 8. 2004. *Design of structures for earthquake resistance-Part 1: General rules, seismic actions and rules for buildings*. Brussels: CEN.

GB 50011-2010. 2010. *Code for seismic design of buildings*. Beijing, China: The Ministry of Housing and Urban-Rural Development of the People's Republic of China. China Architecture and Building Press.

Greco, R., A. Fiore, and B. Briseghella. 2018b. Influence of soil type on damping reduction factor: A stochastic analysis based on peak theory. *Soil Dynamics and Earthquake Engineering* 104: 365–68.

Greco, R., A. Fiore, G. C. Marano, and B. Briseghella. 2018a. Effects of excitation bandwidth on damping reduction factor. *Journal of Earthquake Engineering* 25 649–76.

Greco, R., I. Vanzi, D. Lavorato, and B. Briseghella. 2019. Seismic duration effect on damping reduction factor using random vibration theory. *Engineering Structures* 179: 296–309.

Hao, A., D. Zhou, Y. Li, and H. Zhang. 2011. Effects of moment magnitude, site conditions and closest distance on damping modification factors. *Soil Dynamics and Earthquake Engineering* 31: 1232–47.

Hatzigeorgiou, G. D. 2010. Damping modification factors for SDOF systems subjected to near-fault, far-fault and artificial earthquakes. *Earthquake Engineering & Structural Dynamics* 39: 1239–58.
Hubbard, D. T., and G. P. Mavroeidis. 2011. Damping coefficients for near-fault ground motion response spectra. *Soil Dynamics and Earthquake Engineering* 31: 401–17.
Japanese Seismic Design Code. 2000. Technical standard for structural calculation of response and limit strength of buildings. Notification No. 1457–2000, Ministry of Land, Infrastructure and Transport. (In Japanese).
Lin, Y. Y., E. Miranda, and K. C. Chang. 2005. Evaluation of damping reduction factors for estimating elastic response of structures with high damping. *Earthquake Engineering & Structural Dynamics* 34: 1427–43.
Lin, Y. Y., and K. C. Chang. 2003. Study on damping reduction factor for buildings under earthquake ground motion. *Journal of Structural Engineering* 129: 206–14.
Lin, Y. Y., and K. C. Chang. 2004. Effects of site classes on damping reduction factors. *Journal of Structural Engineering* 130 (11): 1667–75.
Lin, Y. Y. 2007. Statistical study on damping modification factors adopted in Taiwan's seismic isolation design code by using the 21 September 1999 Chi-Chi earthquake, Taiwan. *Engineering Structures* 29: 682–93.
Liu, L., and S. Pezeshk. 1999. An improvement on the estimation of pseudoresponse spectral velocity using RVT method. *Bulletin of the Seismological Society of America* 895: 1384–89.
Mentrasti, L. 2008. Estimate of spectral and pseudo-spectral acceleration proximity. *Engineering Structures* 30: 2338–46.
Mollaioli, F., L. Liberatore, and A. Lucchini. 2014. Displacement damping modification factors for pulse-like and ordinary records. *Engineering Structures* 78: 17–27.
Naeim, F., and J. M. Kelly. 1999. *Design of seismic isolated structures. From theory to practice*. New York: John Wiley and Sons.
Nagao, K., and J. Kanda. 2015. Estimation of damping correction factors using duration defined by standard deviation of phase difference. *Earthquake Spectra* 31: 761–83.
National Research Institute for Earth Science and Disaster Resilience (NIED). 1995. Strong motion seismograph networks (K-NET, KIK-net). Accessed December 2020. http://www.kyoshin.bosai.go.jp/kyoshin/
NEHRP. 2000. *Recommended provisions for seismic regulations for new buildings and other structures*. Washington DC: Federal Emergency Management Agency.
Newmark, N. M., and W. J. Hall. 1982. *Earthquake spectra and design EERI monograph series*. Oakland, CA: Earth Eng Research Inst.
Nigam, N., and P. Jennings. 1969. Calculation of response spectra from strong-motion earthquake records. *Bulletin of the Seismological Society of America* 59 (2): 909–22.
Palermo, M., S. Silvestri, and T. Trombetti. 2016. Stochastic-based damping reduction factors. *Soil Dynamics and Earthquake Engineering* 80: 168–76.
Pu, W., K. Kasai, E. K. Karoki, and B. Huang. 2016. Evaluation of the damping modification factor for structures subjected to near-fault ground motions. *Bulletin of Earthquake Engineering* 14: 1519–44.
Ramirez, O. M., M. C. Constantinou, C. A. Kircher, A. S. Whittaker, M. W. Johnson, J. D. Gomez, and C. Z. Chrysostomou. 2000. Development and evaluation of simplified procedures for analysis and design of buildings with passive energy dissipation systems. New York: Multidisciplinary Center for Earthquake Engineering Research (MCEER), University of New York at Buffalo; ReportNo: MCEER-00-0010.
Rezaeian, S., Y. Bozorgnia, I. M. Idriss, N. Abrahamson, K. Campbell, and W. Silva. 2014. Damping scaling factors for elastic response spectra for shallow crustal earthquakes in active tectonic regions: "average" horizontal component. *Earthquake Spectra* 30 (2): 939–63.
Sadek, F., B. Mohraz, and M. A. Riley. 2000. Linear procedures for structures with velocity-dependent dampers. *Journal of Structural Engineering* 126 (8): 887–95.
Stafford, P. J., R. Mendis, and J. J. Bommer. 2008. Dependence of damping correction factors for response spectra on duration and numbers of cycles. *Journal of Structural Engineering* 134 (8): 1364–73.
Tolis, S. V., and E. Faccioli. 1999. Displacement design spectra. *Journal of Structural Engineering* 3: 107–25.
Vanmarcke, E. H. 1975. On the distribution of the first-passage time for normal stationary random processes. *Journal of Applied Mechanics* 42: 215–20.
Wang, X., and E. M. Rathje. 2016. Influence of peak factors on site amplification from random vibration theory based site-response analysis. *Bulletin of the Seismological Society of America* 106: 1–14.
Xiang, Y., and Q. L. Huang. 2019. Damping modification factor for the vertical seismic response spectrum: A study based on Japanese earthquake records. *Engineering Structures* 179: 493–511.
Zhang, H. Z., and Y. G. Zhao. 2020. Damping modification factor based on random vibration theory using a source-based ground-motion model. *Soil Dynamics and Earthquake Engineering* 136: 106225.
Zhao, X., Q. Yang, K. Su, J. Liang, J. Zhou, H. Zhang, and X. Yang. 2019. Effects of earthquake source, path, and site conditions on damping modification factor for the response spectrum of the horizontal component from subduction earthquakes. *Bulletin of the Seismological Society of America* 109: 2954–2613.
Zhou, J., K. Tang, H. Wang, and X. Fang. 2014. Influence of ground motion duration on damping reduction factor. *Journal of Earthquake Engineering* 18 (5): 816–30.